Journal of Power Sources 230 (2013) 244–250

Contents lists available at SciVerse ScienceDirect

Journal of Power Sources

journal homepage: www.elsevier.com/locate/jpowsour

A comparative study of state of charge estimation algorithms for $LiFePO_4$ batteries used in electric vehicles

Jiahao Li*, Joaquin Klee Barillas, Clemens Guenther, Michael A. Danzer

Zentrum für Sonnenenergie- und Wasserstoff-Forschung Baden-Württemberg, Lise-Meitner-Str. 24, 89081 Ulm, Germany

HIGHLIGHTS

- An equivalent circuit is used to describe the characteristics of $LiFePO_4$ batteries.
- Three different model-based algorithms are designed to estimate the battery SOC.
- The estimation approaches are verified with two typical driving profiles.
- The system robustness and the convergence behavior of SOC estimators are compared.

ARTICLE INFO

Article history:
Received 18 September 2012
Received in revised form
11 December 2012
Accepted 15 December 2012
Available online 27 December 2012

Keywords:
Lithium-ion battery
State of charge estimation
Extended Kalman filter
Sigma point Kalman filter
Convergence behavior
Robust estimation

ABSTRACT

One of the most important aspects in battery management systems (BMS) in electric vehicles is the state of charge (SOC) estimation. SOC needs to be accurately determined for safety and performance reasons but cannot be measured directly due to the flatness and hysteresis of the open circuit voltage (OCV) curve of Lithium-ion chemistries as $LiFePO_4$. The classical approach of current integration (Coulomb counting) cannot solve the problems of accumulative error and inaccurate initial values, thus advanced estimation algorithms are applied to determine the sate of charge. In this work, three model-based state observer designs including Luenberger observer, Extended Kalman Filter (EKF) and Sigma Point Kalman Filter (SPKF) are carried out and studied. These estimation approaches are verified using measurement data acquired from commercial $LiFePO_4$ cells. In addition, computational tests analyze the systems performances in terms of tracking accuracy, estimation robustness against temperature uncertainty, sensor drift, and convergence behavior with an initial SOC offset.

1. Introduction

Recently, with more emphasis on environment-friendly vehicles, the use of electric powered transportation is increasing. For automotive industry the lithium-ion energy storage system is currently considered as the best alternative to meet high specific energy and specific power demands of electric vehicles (EVs). Based on current research and development, $LiFePO_4$ (LFP) as active material of the positive electrode is more stable and safer as other cell chemistries under abusive operating conditions [1]. Together with its low cost and long lifespan, LFP is a favorable choice as cathode material in EV applications.

The battery pack of an EV is controlled by a battery management system (BMS). In complex and dynamic vehicle operation conditions, a good BMS is required to provide accurate knowledge of the battery's state of charge (SOC). This information reflects the remaining capacity that can be drawn from the battery pack and is used to ensure an optimum control of charging and discharging processes [2]. However, several factors for SOC determination for LFP-batteries such as hysteresis phenomena, flat characteristic of open-circuit-voltage (OCV) over SOC, and limited voltage measurement accuracy can result in SOC estimation errors.

A widely used method to estimate SOC is the Coulomb counting approach [3,4], which samples the battery current and computes the accumulated charge and discharge to estimate SOC. This approach is simple and inexpensive to implement. However, it faces drawbacks such as accumulated measurement error and inaccurate initial SOC values. Other methods described in [5], such as discharge test or internal resistant characteristic, are usually considered as laboratory methods. Additionally, the artificial neural networks, e.g. [6] can simulate

* Corresponding author. Tel.: +49 731 9530 537; fax: +49 731 9530 599.
E-mail addresses: jiahao.li@zsw-bw.de, jiahao.li@gmx.de (J. Li).

0378-7753/$ – see front matter © 2012 Elsevier B.V. All rights reserved.
http://dx.doi.org/10.1016/j.jpowsour.2012.12.057

the complicated battery dynamic. However, its performance is sensitive to training data. Therefore, it is not appropriate for the battery online application.

Further developed strategies for battery SOC estimation are model-based techniques. State estimation with Luenberger observer has already been analyzed [7]. Later on, a Kalman Filter (KF) approach with its knowledge about statistical characteristics of process and measurement noise is intensively studied [8–10]. Extended Kalman Filter (EKF) and Sigma Point Kalman Filter (SPKF) are two improvements to the classical KF which are investigated for nonlinear systems. EKF uses the first order Taylor series to transform the nonlinear system into a linear system [11] while the second approach uses the unscented transformation to approximate the probability density function of the nonlinear system with series deterministic points [12].

This work presents a survey and a comparative study of the model-based SOC estimation approaches above with focus on estimation robustness. At first, the considered estimation algorithms are separately studied. Based on the theoretical and practical analysis, this work determines the optimal choice to estimate dynamic SOC behavior for LFP cells.

2. Description of cell model

A battery equivalent circuit used for model-based state estimation design is shown in Fig. 1.

The steady state cell behavior is characterized by the OCV voltage. It refers to the potential difference between two electrodes in an open circuit. At a certain temperature, the relationship between SOC and OCV is obtained through measurement and can be established for the state estimation using a nonlinear function or lookup tables [11,13]. The dynamic cell behavior is described by an ohmic resistance R_0 with two RC elements in series with a short and a long time constant. The parameters can be identified using nonlinear least-squares methods, which minimize the error between the model output and experimental data until a predefined error bound is reached [15,16]. Based on the Coulomb counting law and the linear differential equation of RC circuits, the discrete-time dynamic equations of the cell model and the cell voltage can be expressed by

$$\mathrm{SOC}(k) = \mathrm{SOC}(k-1) + I(k)\cdot\eta\cdot\Delta t/C_\mathrm{N}, \tag{1}$$

$$V_1(k) = (1-\Delta t/(R_1C_1))\cdot V_1(k-1) + I(k)\cdot\Delta t/C_1, \tag{2}$$

and

$$V_2(k) = (1-\Delta t/(R_2C_2))\cdot V_2(k-1) + I(k)\cdot\Delta t/C_2, \tag{3}$$

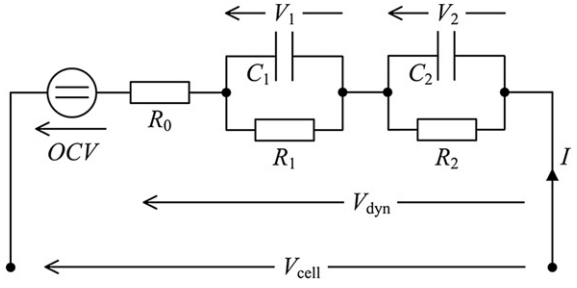

Fig. 1. Cell equivalent circuit model with open-circuit-voltage, cell ohmic resistant R_0, resistances of RC circuits R_1 and R_2 as well as capacitances of RC circuits C_1 and C_2.

where k is the discrete-time index, V_1 and V_2 the capacitor voltages, η the columbic efficiency, and C_N the discharge capacity of the battery. Additionally, charging current is defined as a positive value. Hence, the cell voltage is calculated as

$$V_\mathrm{cell}(k) = \mathrm{OCV}(\mathrm{SOC}(k)) + V_1(k) + V_2(k) + R_0I(k). \tag{4}$$

By referring to Fig. 1 and considering the current I as the model input, the state vector of the cell model $\mathbf{x}_k$ can be chosen as

$$\mathbf{x} = [\mathrm{SOC}, V_1, V_2]^T. \tag{5}$$

In order to facilitate the application of model-based estimation algorithms, the system equations from (1) to (4) need to be translated into a discrete-time state space form

$$\mathbf{x}_k = \mathbf{A}\,\mathbf{x}_{k-1} + \mathbf{B}\;u_k, \quad \mathbf{x}(t_0) = \mathbf{x}_0, \tag{6}$$

and

$$z_k = V_\mathrm{cell} = g(\mathbf{x}_{k-1}, u_k), \tag{7}$$

where $\mathbf{A}$ is the dynamic matrix, $\mathbf{B}$ the input matrix, $g(\cdot)$ the nonlinear process output model, u the model input, and $\mathbf{x}_0$ the initial state at time $t = t_0$.

3. Proposed methodology

Three closed loop state observers are investigated in this work. The general structure of battery SOC estimation is shown in Fig. 2.

The principle of SOC observation is to generate the cell voltage from the state estimator and to compare it with the measurement value. By feeding back this difference into the model, the predicted battery SOC can be corrected with a so-called feedback gain matrix. This matrix can be determined by the following methods:

3.1. Luenberger observer

The Luenberger observer is widespread for linear deterministic dynamic systems in the industry because of its simple implementation and tuning of the observer gain. Based on the system knowledge, the Luenberger observer is usually designed with a constant feedback gain. Therefore, in spite of a nonlinear output function (4), the state correction is proportional to the voltage residual e_k

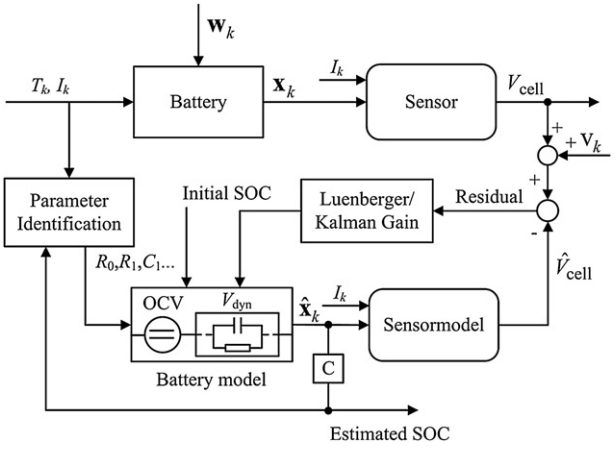

Fig. 2. The structure of model based battery SOC estimation with cell temperature T, terminal voltage V_cell, input u, real states $\mathbf{x}$, and estimated states $\hat{\mathbf{x}}$.

$$e_k = z_k - \hat{z}_k, \tag{8}$$

and

$$\hat{\mathbf{x}}_k = \mathbf{A}\,\mathbf{x}_{k-1} + \mathbf{B}\,u_k + \mathbf{k}\,e_k, \tag{9}$$

with the Luenberger gain vector k.

Note that the OCV of LFP cells is very flat over a wide SOC range. The residual e_k calculated between measured and modeled cell voltage may not correspond to the actual SOC variation due to the measurement noise. Therefore, two Kalman based filter algorithms are further used for this nonlinear estimation problem.

3.2. Extended Kalman filter

The Kalman filtering is an optimal recursive solution to the linear Gaussian problem. A Kalman filter estimates the state of a dynamic system with a linear process model and measurement model [17]. To nonlinear problems, the most well known inference of the Kalman Filter framework is the extended Kalman filter (EKF). Compared to a linear state space description in (6), the general framework of a discrete-time nonlinear system with noise input is given by

$$\mathbf{x}_k = \mathbf{f}(\mathbf{x}_{k-1}, u_k) + \mathbf{w}_k, \quad \mathbf{x}(t_0) = \mathbf{x}_0, \tag{10}$$

and

$$z_k = g(\mathbf{x}_{k-1}, u_k) + \mathrm{v}_k, \tag{11}$$

where $\mathbf{f}(\cdot)$ and $g(\cdot)$ are the nonlinear process model and the measurement model. Vector $\mathbf{w}_k$ represents the system noise and v_k the measurement noise. Both $\mathbf{w}_k$ and v_k are assumed to be uncorrelated, zero-mean Gaussian white sequences and their covariances are known as $\mathbf{Q}_k$ and r_k respectively [17]. The EKF algorithm could be mathematically expressed as

- Prediction update

$$\hat{\mathbf{x}}_k^- = \mathbf{f}(\mathbf{x}_{k-1}, u_k, \mathbf{x}_0), \tag{12}$$

$$\mathbf{P}_k^- = \mathbf{A}_k\mathbf{P}_{k-1}\mathbf{A}_k^T + \mathbf{w}_k\mathbf{Q}_{k-1}\mathbf{w}_k^T, \tag{13}$$

and

- Measurement update

$$\mathbf{k}_k = \mathbf{P}_k^-\mathbf{C}_k^T\left(\mathbf{C}_k\mathbf{P}_k^-\mathbf{C}_k^T + \mathrm{v}_k\mathrm{r}_k\mathrm{v}_k^T\right)^{-1}, \tag{14}$$

$$\hat{\mathbf{x}}_k = \hat{\mathbf{x}}_k^- + \mathbf{k}_k(z_k - g(\hat{\mathbf{x}}_k^-, u_k)), \tag{15}$$

and

$$\mathbf{P}_k = (\mathbf{I} - \mathbf{k}_k\mathbf{C}_k)\mathbf{P}_k^-, \tag{16}$$

where $\mathbf{P}_k$ is the error covariance of the state estimation, $\hat{\mathbf{x}}_k^-$ the priori state estimate at step k and $\hat{\mathbf{x}}_k$ the posterior state estimate. $\mathbf{A}_k$, $\mathbf{B}_k$ are defined as the Jacobian matrices

$$\mathbf{A}_k = \left.\frac{\partial \mathbf{f}}{\partial \mathbf{x}}\right|_{\mathbf{x}=\hat{\mathbf{x}}_k^-}, \quad \mathbf{C}_k = \left.\frac{\partial g}{\partial \mathbf{x}}\right|_{\mathbf{x}=\hat{\mathbf{x}}_k^-}, \tag{17}$$

Notice that the key idea underlying the EKF approach is the linearization. It approximates the nonlinear function utilizing the first order Taylor expansion by the partial derivative. A detailed explanation for EKF is given in [18]. Accordingly, one important limitation of the EKF is its local linear expansions. For the battery SOC estimation, because of the stepwise flatness and the hysteresis effect of the OCV and SOC curve the measurement model is inherently nonlinear. When the degrees of system uncertainty or nonlinearity are significant, these approximations of the EKF can result in large estimation errors [12].

3.3. Sigma point Kalman filter

The Sigma Point Kalman Filter (SPKF) or unscented Kalman Filter (UKF) addresses the approximation issues of the EKF. Fig. 3 illustrates the linearization applied by the sampling methods, EKF and SPKF. Instead of local linearization, the SPKF captures the statistical distribution of the nonlinear system using deterministic sampling (so-called sigma points).

In the general case, these sigma points are located at the mean and symmetrically along the main axes of the covariance [18]. The unscented Kalman Filter can be summarized as follows

- Calculating sigma points with mean $\mathbf{x}_{k-1}$ and covariance $\mathbf{P}_k$

$$\boldsymbol{\chi}^{[0]} = \mathbf{x}_{k-1}, \tag{18}$$

$$\boldsymbol{\chi}^{[i]} = \mathbf{x}_{k-1} + \left(\sqrt{(n+\lambda)\mathbf{P}_k}\right)_i, \quad i = 1, 2, \ldots, n, \tag{19}$$

and

$$\boldsymbol{\chi}^{[i]} = \mathbf{x}_{k-1} - \left(\sqrt{(n+\lambda)\mathbf{P}_k}\right)_{i-n}, \quad i = n+1, n+2, \ldots, 2n, \tag{20}$$

where n is the dimension of the state vector. The number of sigma points $\boldsymbol{\chi}$ is calculated as $2n + 1$. The parameter λ is expressed as

$$\lambda = \alpha^2(n + \kappa) - n, \tag{21}$$

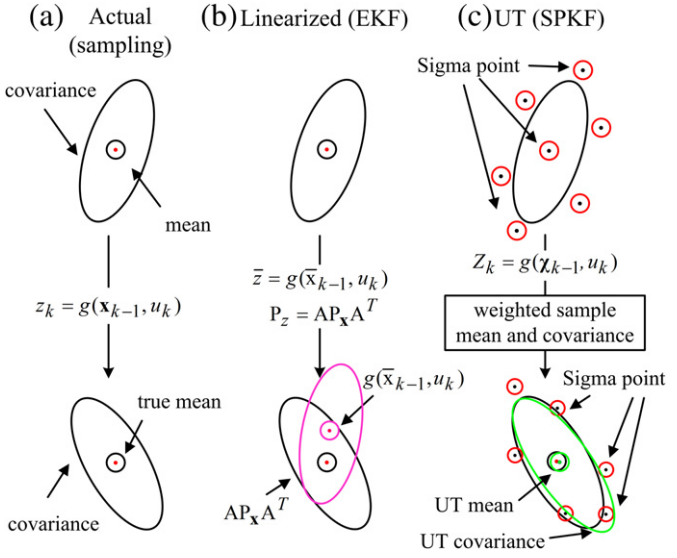

Fig. 3. Linearized transformation of the EKF and unscented transformation (UT) of the sigma point approach [18].

where α ($0 \leq \alpha \leq 1$) and κ (default choice is $\kappa = 0$) are tuning parameters that determine the distribution of the sigma points spreaded from the mean [19].

- Calculating weights associated with each sigma point

$$\mathbf{w}_m^{[0]} = \frac{\lambda}{n+\lambda}, \tag{22}$$

$$\mathbf{w}_c^{[0]} = \frac{\lambda}{n+\lambda} + \left(1 - \alpha^2 + \beta\right), \tag{23}$$

and

$$\mathbf{w}_m^{[i]} = \mathbf{w}_c^{[i]} = \frac{1}{2n+2\lambda}, \quad i = 1, 2, \ldots, 2n, \tag{24}$$

where $\mathbf{w}_m$ and $\mathbf{w}_c$ are sets of weighting matrices. The parameter β can be used to incorporate the higher order knowledge about the distribution. For a Gaussian distribution, $\beta = 2$ is the optimal choice [19].

- Prediction update

Update each sigma point through the nonlinear dynamic equation to predict the system state as

$$\widehat{\boldsymbol{\chi}}_k^* = \mathbf{f}(\boldsymbol{\chi}_{k-1}, u_k), \tag{25}$$

$$\widehat{\overline{\mathbf{x}}}_k^- = \sum_{i=0}^{2n} \mathbf{w}_m^{[i]}\, \widehat{\boldsymbol{\chi}}_k^{*[i]}, \tag{26}$$

and

$$\mathbf{P}_k^- = \sum_{i=0}^{2n} \mathbf{w}_c^{[i]} \left(\widehat{\boldsymbol{\chi}}_k^{*[i]} - \widehat{\overline{\mathbf{x}}}_k^-\right)\left(\widehat{\boldsymbol{\chi}}_k^{*[i]} - \widehat{\overline{\mathbf{x}}}_k^-\right)^T + \mathbf{w}_k \mathbf{Q}_{k-1} \mathbf{w}_k^T, \tag{27}$$

where the prior state estimation $\widehat{\overline{\mathbf{x}}}_k^-$ is derived from the weighted mean of the sigma points vector $\widehat{\boldsymbol{\chi}}_k^*$. The prior covariance matrix $\mathbf{P}_k^-$ is estimated as the weighted sum of the squared distances of all the sigma points from $\widehat{\overline{\mathbf{x}}}_k^-$.

- Measurement update

Update each sigma point through the nonlinear measurement equation to predict the measurement value as

$$\widehat{Z}_k^* = g\left(\widehat{\boldsymbol{\chi}}_k^-, u_k\right), \tag{28}$$

and

$$\widehat{\overline{z}}_k = \sum_{i=0}^{2n} \mathbf{w}_m^{[i]}\, \widehat{Z}_k^{*[i]}. \tag{29}$$

After the prediction step, the estimates of the system states and covariance are defined by

$$\widehat{\mathbf{x}}_k = \widehat{\overline{\mathbf{x}}}_k^- + \mathbf{k}_k\left(z_k - \widehat{\overline{z}}_k\right), \tag{30}$$

and

$$\mathbf{P}_k = \mathbf{P}_k^- - \mathbf{k}_k \mathbf{P}_z \mathbf{k}_k^T, \tag{31}$$

where

$$\mathbf{k}_k = \mathbf{P}_{xz}^- \mathbf{P}_z^{-1}, \tag{32}$$

$$\mathbf{P}_z = \sum_{i=0}^{2n} \mathbf{w}_c^{[i]} \left(\widehat{Z}_k^{*[i]} - \widehat{\overline{z}}_k\right)\left(\widehat{Z}_k^{*[i]} - \widehat{\overline{z}}_k\right)^T + \mathrm{v}_k \mathrm{r}_k \mathrm{v}_k^T, \tag{33}$$

and

$$\mathbf{P}_{xz}^- = \sum_{i=0}^{2n} \mathbf{w}_c^{[i]} \left(\widehat{\boldsymbol{\chi}}_k^{*[i]} - \widehat{\overline{\mathbf{x}}}_k\right)\left(\widehat{Z}_k^{*[i]} - \widehat{\overline{z}}_k\right)^T. \tag{34}$$

4. Experimental details

In the present work, an LFP pouch cell with high specific energy, having a nominal capacity of 20 Ah and a nominal voltage of 3.3 V, is used for the comparison study of the SOC estimation algorithms. The SOC verification tests are carried out on a BaSyTec test bench with 0–10 V voltage range and currents up to 250 A. The accuracy of both voltage and current measurement is within 0.05% of the full scale range, and the resolution within 0.003%. During the test, the cell is located in a climatic chamber ESPEC PU-3KP (temperature range −40 °C–100 °C, accuracy: ±0.5 °C) and the cell ambient temperature is constantly held at 30 °C.

In order to evaluate the SOC estimation approaches, two typical driving profiles, the New European Driving Cycle (NEDC) and the ARTEMIS cycle [14], are applied. The current sequences are derived from these driving profiles and depicted in Fig. 4. The first test with one NEDC current load takes approximately 20 min. The initial SOC is adjusted to 80% SOC. In the second test, the entire operating range of the cell is utilized. The ARTEMIS load cycle, started with 90% SOC, is repeated until the cell voltage reaches its limitation (1 min rest between two cycles). Data points are collected at 50 Hz during the tests.

The nonlinear battery model in Matlab/Simulink incorporates the measured data including voltage, current, and temperature from the test bench and estimates the SOC value with the presented approaches. The SOC performances are compared with the current integration which serves as the actual SOC behavior.

5. Results and discussion

5.1. NEDC with 80% start SOC

Figs. 5 and 6 demonstrate the results of the proposed estimation approaches with the NEDC, when the SOC is correctly initialized to 80%. Tracking for SOC behavior is shown in Fig. 5. Fig. 6 illustrates the cell terminal voltage estimation. Generally, the estimated value is consistent with the measured one. Nevertheless, using nonlinear algorithms, SOC can be estimated more accurately (error less than 1%) in comparison with 2% error with the Luenberger observer.

Note that the estimation errors start at zero and diverge slowly away from the true behavior. Although the voltage estimation error of SPKF is approximately zero (±1 mV in Fig. 6), the uncertainty of the battery model could result in the slight SOC divergence.

5.2. ARTEMIS driving cycle with observable start SOC and unobservable start SOC

In the second test regime the SOC algorithms are performed with the ARTEMIS driving cycle including a more dynamic current

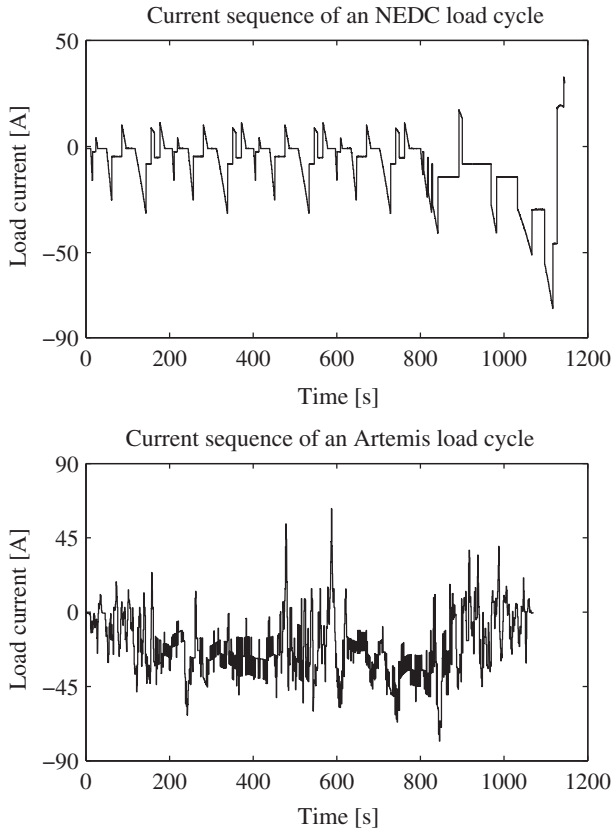

Fig. 4. Applied current sequences of NEDC and ARTEMIS driving profiles utilized for the SOC estimation.

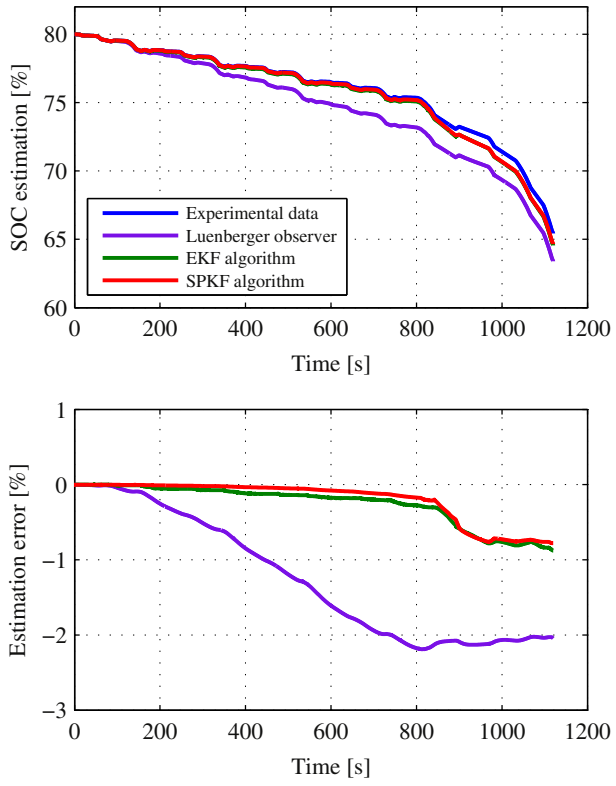

Fig. 5. Comparison of SOC behavior and estimation error under NEDC.

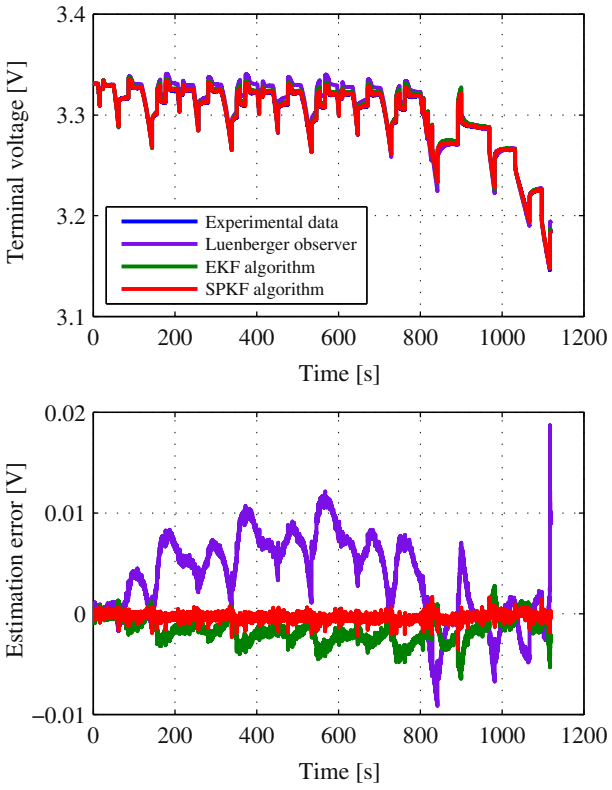

Fig. 6. Comparison of estimated terminal voltage and estimation error under NEDC.

load for the entire operation range. Fig. 7 depicts the estimation results with both observable and unobserverable start SOC.

The achieved SOC performances are evaluated by the maximum estimation error and the convergence behavior for incorrect initialization of SOC. When the start SOC is correctly initialized to 90%, all approaches give similar estimation errors (maximum 3% error). However, an observable start SOC usually cannot be guaranteed in practice. By defining a 20% start SOC error, the superior performance of SPKF can be clearly seen. The SPKF enables the fastest convergence rate and stabilization of SOC behavior without remarkable SOC oscillations.

5.3. Temperature uncertainty and sensor drift

Cell temperature is one of the most significant factors impacting both the performance and the useful life of the battery. Because of different sensor positions, battery aging and cooling strategy of BMS, the cell temperature could not be directly or exactly measured. In order to investigate the estimation robustness of proposed approaches, a +3 °C temperature offset and a +4 mV voltage measurement offset are further embedded in the computer simulation.

Simulations are carried out with the same ARTEMIS drive profile starting from 90% initial SOC as for Fig. 7(a). In Fig. 8(a) the simulated temperature is raised with 3 °C, which reduces the model accuracy and changes slightly the SOC-OCV behavior. Fig. 8(b) shows the result with a voltage measurement error. Very close agreement in Fig. 8 is observed, as expected. It can be concluded that the SOC performance with Luenberger observer is more influenced by the measurement accuracy. The estimation error from both situations is enlarged and lasts to the end of the test. In contrast, behaviors of EKF and SPKF are nearly consistent with the measurements from Fig. 7(c).

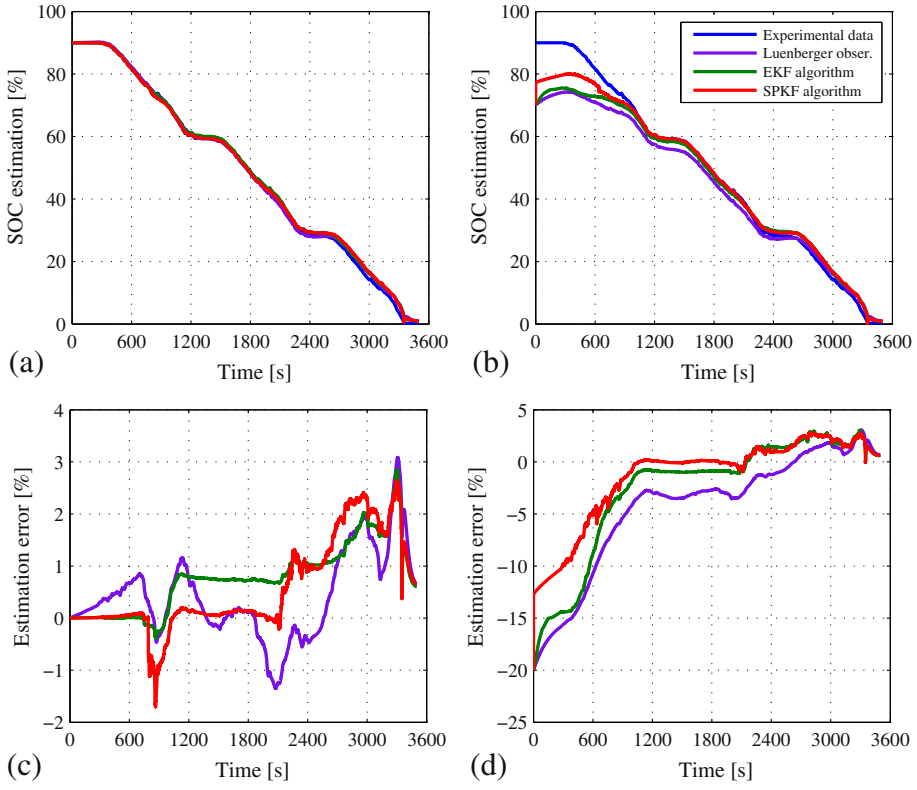

Fig. 7. Comparison of the SOC estimation with observable (a) and unobservable (b) start SOC and corresponding estimation error (c) and (d) for ARTEMIS driving cycle.

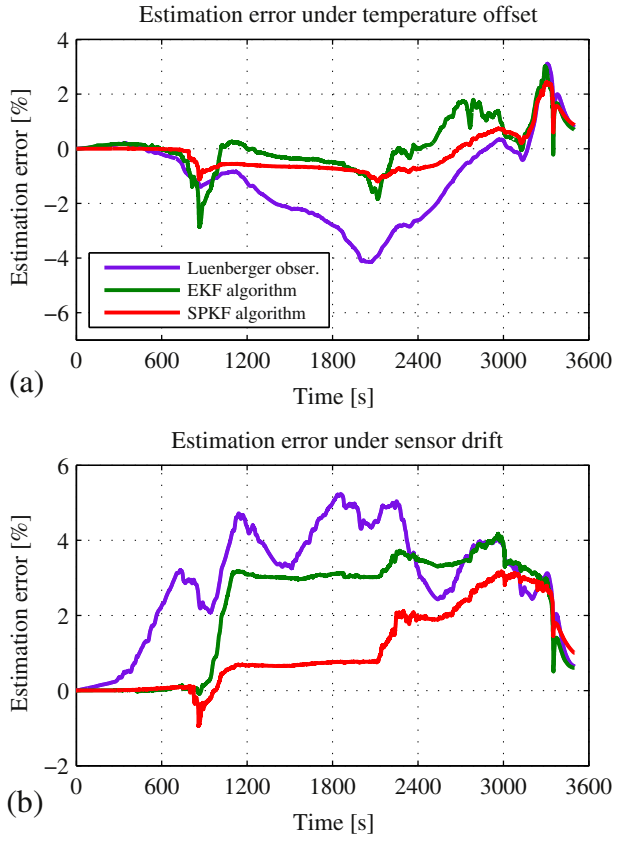

Fig. 8. Comparison of the estimation error with +3 °C temperature offset (a) and +4 mV sensor drift for voltage measurement (b).

Table 1
Root mean square error (RMSE) of different methods in SOC estimation for ARTEMIS driving cycle from 90% SOC.

Methods	Observable start SOC	Unobservable start SOC	Temperature uncertainty	Sensor drift
Luenberger	1.05	7.3	1.8	2.7
EKF	0.95	6.2	0.94	1.8
SPKF	0.96	4.3	0.95	1.6

To summarize, an overview of root mean square errors (RMSE) for each estimation method in terms of considered situations is presented in Table 1. The classical Luenberger observer relies mostly on the accuracy of the battery model, as it can hardly take the model uncertainty and measurement noise into account. EKF is comparatively more accurate than Luenberger method. The difference between EKF and SPKF is mainly reflected in the convergence rate with an unobservable start SOC. For most states, SPKF provides the better SOC estimation results than other approaches.

6. Conclusion

In this work, three model-based algorithms including standard Luenberger observer, EKF, and SPKF are applied to monitor the SOC of an LFP battery. First, an equivalent electrical model is represented to describe the battery electrical behavior. Then, the general formulations of estimation approaches have been studied. Their performances are compared using the measurement data acquired from a commercial LFP cell on a test bench. Simulation results denote the improvement of SPKF for the battery SOC estimation in terms of tracking accuracy, the convergence behavior, and the estimation robustness. In addition, the nonlinear approximation using unscented transformation avoids computing the Jacobian matrix of

EKF (17). Therefore, SPKF can also provide a better numerical stability.

In future work, the algorithms will be implemented on a BMS and thereby be validated under limited achievable computation power and precision of floating point numbers. In a further development stage the underlying battery model will be extended taking battery aging (capacity fade and resistance rise) into account. Therewith the performance of the algorithms over the lifetime of the battery will be further improved.

References

[1] M. Safari, C. Delacourt, Aging of a commercial graphite/$LiFePO_4$ cell, J. Electrochem. Soc. 158 (10) (2011) 1123–1135.
[2] B. Pattipati, K. Pattipati, J. Christopherson, Automotive Battery Management System, IEEE Autotestcon, Salt Lake City, USA, 2008.
[3] J. Aylor, B. Johnson, A battery state-of-charge indicator for electric wheelchairs, IEEE Trans. Ind. Electron. 39 (1992) 398–409.
[4] T. Liu, D. Chen, Design and implementation of a battery charger with a state-of-charge estimator, Int. J. Electron. 87 (2000) 211–226.
[5] S. Pillter, M. Perrin, A. Jossen, Methods for state of charge determination and their applications, J. Power Sources 96 (2001) 113–120.
[6] B. Cheng, Z. Bai, State of charge estimation based on evolutionary neural network, Energy Convers. 49 (2008) 2788–2794.
[7] X. Hu, F. Sun, Y. Zou, Estimation of state of charge of a lithium-ion battery pack for electric vehicles using an adaptive Luenberger observer, Energies 3 (2010) 1586–1603.
[8] J. Wang, J. Guo, L. Ding, An adaptive Kalman filtering based State of Charge combined estimator for electric vehicle battery pack, Energy Convers. Manag. (2009) 3182–3186.
[9] Gregory L. Plett, Extended Kalman filtering for battery management systems of LiPB-based HEV battery packs part 2, J. Power Sources 134 (2004) 277–292.
[10] Z. Chen, S. Qiu, M.A. Masrur, Y. Murphey, Battery State of Charge Estimation Based on a Combined Model of Extended Kalman Filter and Neural Networks, International Joint Conference on Neural Networks, 2011, pp. 2156–2163.
[11] M. Roscher, O. Bohlen, D. Sauer, Reliable state estimation of multicell lithium-ion battery systems, IEEE Trans. Energy Convers. 3 (2011) 737–743.
[12] R. Merwe, E. Wan, Sigma-Point Kalman Filters for Nonlinear Estimation and Sensor-Fusion – Applications to Integrated Navigation, Navigation & Control Conference, Rhode Island, USA, 2004.
[13] J. Kim, G. Seo, OCV Hysteresis Effect-Based SOC Estimation in Extended Kalman Filter Algorithm for a $LiFePO_4$/C Cell, IEEE Electric Vehicle Conference, 2012, pp. 1–5.
[14] M. Andre, The ARTEMIS European driving cycles for measuring car pollutant emissions, J. Power Sources 334 (2004) 73–84.
[15] Gregory L. Plett, Extended Kalman filtering for battery management systems of LiPB-based HEV battery packs part 1, J. Power Sources 134 (2004) 252–261.
[16] V. Ramadesigan, V. Boovaragavan, M. Arabandi, Parameter estimation and capacity fade analysis of lithium-ion batteries using first-principles-based efficient reformulated models, J. Electrochem. Soc. 19 (16) (2009) 11–19.
[17] B. Ristic, S. Arulampalam, N. Gordon, Beyond the Kalman Filter, Artech House, Boston, 2004.
[18] S. Thrun, W. Burgasrd, D. Fox, Probabilistic Robotics. Massachusetts Institute of Technology, The MIT Press, USA, 2006.
[19] R. Kandepu, B. Foss, L. Iamsland, Applying the unscented Kalman filter for nonlinear state estimation, J. Process Control 18 (2008) 753–768.